Direct Evidence of Fe^{2+}-Fe^{3+} Charge Ordering in the Ferrimagnetic Hematite-Ilmenite $Fe_{1.35}Ti_{0.65}O_{3-\delta}$ Thin Films

L. Bocher,[1] E. Popova,[2] M. Nolan,[3] A. Gloter,[1] E. Chikoidze,[2] K. March,[1] B. Warot-Fonrose,[4] B. Berini,[2] O. Stéphan,[1] N. Keller,[2] and Y. Dumont[2,*]

[1]*Laboratoire de Physique des Solides, Bâtiment 510, UMR 8502, Université Paris Sud XI and CNRS, 91405 Orsay, France*
[2]*Groupe d'Etudes de la Matière Condensée (GEMaC), UMR 8635, Université de Versailles St Quentin en Yvelines and CNRS, 78035 Versailles, France*
[3]*Tyndall National Institute, University College Cork, Lee Maltings, Cork, Ireland*
[4]*Centre d'Elaboration de Matériaux et d'Etudes Structurales (CEMES), UPR 8011, CNRS, 31055 Toulouse, France*
(Received 30 March 2013; published 14 October 2013)

In this Letter we highlight direct experimental evidence of Fe^{2+}-Fe^{3+} charge ordering at room temperature in hematite-ilmenite $Fe_{1.35}Ti_{0.65}O_{3-\delta}$ epitaxial thin films grown by pulsed laser deposition, using aberration-corrected scanning transmission electron microscopy coupled to high-resolution energy electron-loss spectroscopy. These advanced spectromicroscopy techniques demonstrate a strong modulation of the Fe^{2+} valence state along the c axis. Density functional theory calculations provide crucial information on the key role of oxygen vacancies in the observed charge distributions. Their presence at significant levels leads to the localization of extra electrons onto reduced Fe^{2+} sites, while Ti remains solely +4. The magnetic and transport properties of these films are reviewed in the light of the present results regarding their ferrimagnetic character correlated with the Fe^{2+} modulation and their semiconducting behavior interpreted by an Efros-Shklovskii variable-range hopping conduction regime via Fe^{2+} and Fe^{3+} centers. The experimental evidence of only one type of mixed valence state, i.e., Fe^{2+} and Fe^{3+}, in the $Fe_{2-x}Ti_xO_{3-\delta}$ system will thus help to interpret further the origin of its geomagnetic properties and to illuminate fundamental issues regarding its spintronic potential.

A strong interplay between charge, lattice, orbital, and spin degrees of freedom exists in transition-metal oxides, yielding the emergence of a large spectrum of functionalities such as high-temperature superconductivity [1], metal-insulator transition [2], thermoelectricity [3], and recently multiferroicity [4]. Mixed-valence states of $3d$ transition metals act as the driving force in such electronic and magnetic interactions. Valence state modulations can also originate from variations in the oxygen content. Recently, new physical effects were revealed at the interfaces of artificial heterostructures made from complex oxides, such as a 2D electron gas at the interface of two insulators ($SrTiO_3$/$LaAlO_3$) or interface-induced magnetoelectric coupling at a ferroelectric-ferromagnetic interface ($BaTiO_3$/Fe) [5,6]. These advances demonstrate how precise knowledge and control of atomic and electronic structures are pivotal in the design of novel physical properties [7].

In this Letter, we focus on a solid solution based on the hematite-ilmenite system (HI), $Fe_{2-x}Ti_xO_{3-\delta}$, which is of great interest (1) in geomagnetism and frustrated magnetism [8], and (2) as a potential spintronic material [9]. In geomagnetism, the magnetic properties of HI are influenced either by nanoscale microstructures associated with spinodal decomposition and cation ordering or by the presence of structural antiphase domains (APDs) inducing a self-reversed thermoremanent magnetization [10]. Regarding

its potential spintronic applications, several theoretical *ab initio* calculations of spin-resolved density of states predict spin polarization either with delocalized electronic states at the Fermi level, or more localized ones, depending strongly on whether strong electronic correlations are considered [11,12]. These works have stimulated several experimental studies on epitaxial $Fe_{2-x}Ti_xO_{3-\delta}$ thin films [13,14] showing a strong structure-property relationship among oxygen-cation stoichiometry, cationic ordering, and magnetic and semiconducting properties [13–16]. Both α-Fe_2O_3 and $FeTiO_3$ end members crystallize in the corundum structure, $R\overline{3}c$ and $R\overline{3}$, respectively [17]. The hematite, α-Fe_2O_3, presents an axial symmetry along the c axis where $3O^{2-}$ layers alternate with $2Fe^{3+}$ ones. Up to 950 K, the magnetic moments are ferromagnetically (FM) coupled inside Fe layers and antiferromagnetically (AFM) coupled between subsequent layers with a small canting [18]. In ilmenite, $FeTiO_3$, Fe^{2+} and Ti^{4+} are octahedrally coordinated by oxygen and partitioned into layers along the c axis, yielding an AFM coupling between FM layers characterized by a Néel temperature of 58 K [19]. Their solid solutions, $Fe_{2-x}Ti_xO_3$, present either the ordered ($R\overline{3}$) or the disordered ($R\overline{3}c$) phase, depending on the cationic arrangement which influences their magnetic and transport properties. However, to our knowledge, no direct evidence of cationic and charge orderings has been presented to date in these complex systems.

Recent technological breakthroughs in electron spectro-microscopy techniques have paved the way toward localizing single atom positions [20] and acquiring 2D elemental maps at subangstrom resolution over large unit cells [21,22]. High-energy-resolution electron energy-loss spectroscopy (EELS) can probe the local bonding environment and the electronic structure of nanostructured materials. The $L_{2,3}$ transition-metal and O K near-edge structures present a strong sensitivity to coordination and hybridization geometries [23], structural distortions [24], and valence state modulations [25]. Combining this information with imaging capabilities in a scanning transmission electron microscope (STEM) yields direct access to the electronic structure down to the atomic scale. Tan *et al.* recently mapped the Mn^{2+}-Mn^{3+} ordering in the binary model system Mn_3O_4 [25]. While this proof of concept opens new horizons for direct visualization of charge ordering mechanisms—with potential for new fundamental insights in condensed matter physics—valence state mapping in more complex transition-metal oxides composed of several cations, each of which has different possible valence states, remains an as-yet unresolved challenge.

Density functional theory (DFT) is a powerful tool to understand further the physical properties of complex materials. Approaches beyond standard approximate DFT functionals have become more accurate in treating the difficult situation of "strongly correlated systems," particularly $3d$ metal oxides, and can be used with confidence to investigate complex transition-metal oxides [26].

In this Letter, we present new results on the atomic and electronic structures of APDs in oxygen deficient $Fe_{1.35}Ti_{0.65}O_{3-\delta}$ (FTO) thin films and provide unambiguous evidence for the Fe^{2+}-Fe^{3+} charge ordering using an atomically resolved real-space spectroscopy technique, i.e., STEM-EELS. DFT results confirm the key role of oxygen vacancies in the local Fe valence state distributions. Finally, both magnetic and hopping charge transport properties of FTO are interpreted in the light of the newly confirmed charge distribution mechanism.

The relaxed 100-nm-thick $Fe_{1.35}Ti_{0.65}O_{3-\delta}$ (FTO) thin films were epitaxially grown by pulsed laser deposition (PLD), under 10^{-7} m Torr oxygen partial pressure, onto α-Al_2O_3(0001) substrates. Details of sample growth can be found elsewhere [16,27]. Electron microscopy studies were performed on cross-sectional views of α-Al_2O_3($1\bar{2}10$)/FTO thin films [28], using a C_s aberration-corrected STEM, the NION UltraSTEM200 operated at 100 kV and coupled with a high-resolution EEL spectrometer characterized by an energy resolution of 350 meV in the core-loss region (see the Supplemental Material [29]). First principles DFT calculations within the well-known DFT $+ U$ formalism (DFT corrected for on-site Coulomb interactions [30]) were carried out in a three-dimensional periodic plane wave basis set formalism using the VASP code [29,31]. The magnetic

properties were measured by a Quantum Design, Inc., PPMS 9T vibrating sample magnetometer. Ohmic electrical contacts on thin films were made through a self-aligned deposition process with a four-point in-line method. dc electrical conductivity was performed at 80 K $<$ T $<$ 550 K using a custom designed high impedance measurement setup.

The FTO film epitaxially grown onto sapphire is single phase and exhibits a good crystallinity as confirmed by x-ray diffraction (XRD) and *in situ* reflection high-energy electron diffraction experiments (see the Supplemental Material [29]) which also demonstrate the epitaxial relationship of FTO(0001) on Al_2O_3(0001) [27]. The presence of the $(0,0,0, 2n + 1)$ Bragg reflections in the XRD pattern is characteristic of the $R\bar{3}$ symmetry indicating a cation ordering along the [0001] zone axis at the macroscopic scale. The ordered $R\bar{3}$ phase was previously observed in similar $Fe_{2-x}Ti_xO_{3-\delta}$ films grown under identical experimental conditions on different substrates [14,27]. Moreover, higher electrical conductivity values were already reported at room temperature for different $Fe_{2-x}Ti_xO_{3-\delta}$ films grown under low oxygen partial pressure PLD conditions [13,16,27], e.g., for $P_{O_2} = 10^{-7}$ m Torr, $\sigma_{300 K} \sim 1\ \Omega^{-1}\,cm^{-1}$ while for $P_{O_2} = 10^{-1}$ m Torr, $\sigma_{300 K} \sim 10^{-3}\ \Omega^{-1}\,cm^{-1}$; this being associated to the presence of oxygen vacancies.

Here we first investigate the cationic arrangement of the ordered FTO film by mapping its atomic structure at the atomic plane level. EELS experiments were performed on different APDs acquiring simultaneously the high-angle annular dark-field (HAADF) signal with the O K, Fe $L_{2,3}$ and Ti $L_{2,3}$ edges [Figs. 1(a) and 1(b)]. As an example, the atomically resolved elemental mapping presented in Figs. 1(b) highlights clearly the cationic modulation between Fe and Ti cations. Based on the EELS quantification, the cationic ratio mean value determined over the structure is of Fe:Ti = 2.05 (0.04) leading to the general composition $Fe_{1.35}Ti_{0.65}O_{3-\delta}$. More interestingly, two types of cationic ratios can be distinguished along the c axis, and are labeled hereafter (i) Fe-rich planes with a ratio of Fe:Ti = 2.33 (0.04) and (ii) mixed Fe-Ti planes with Fe:Ti = 1.77 (0.04) (see the Supplemental Material [29]). The evidence for cationic ordering in the $R\bar{3}$ FTO phase is here demonstrated for the first time from an elemental spectroscopic signature probed at the atomic plane level. Besides, as previously reported for different $Fe_{2-x}Ti_xO_{3-\delta}$ ($x \geq 0.6$) solid solutions [32], we clearly observed in the HAADF image a contrast variation along the c axis over a large ordered APD [29]. The simulated HAADF image based on the ordered structural model confirms this contrast modulation between brighter and darker HAADF signals, i.e., between Fe-rich and Fe-Ti layers, respectively. These additional findings corroborate the cationic arrangement at the atomic plane level in the present ordered FTO phase.
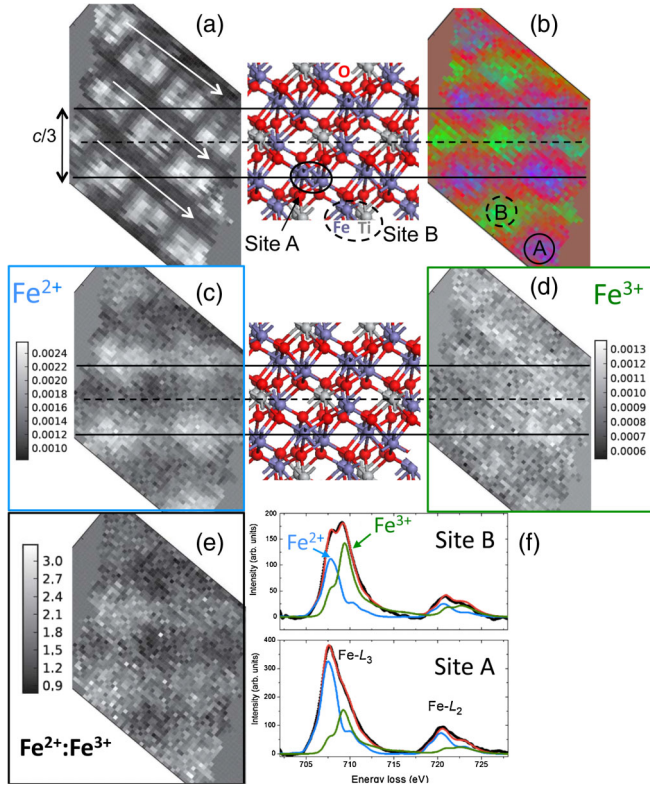
FIG. 1 (color online). (a) HAADF image of the region of interest. (b) Reconstructed map combining the O K, Ti $L_{2,3}$, and Fe $L_{2,3}$ edges (red, green, and blue), (c), (d), and (e) reconstructed maps of the Fe^{2+} and Fe^{3+} spectral weights and the Fe^{2+}:Fe^{3+} ratio, respectively. (f) Examples of linear combinations (red line) of Fe^{2+} (siderite—blue line) and Fe^{3+} (hematite-green line) energy-loss near-edge structure reference spectra fitting experimental ones (black line) acquired on an Fe-rich (site A) or a mixed Fe-Ti (B) site (each single spectrum was acquired in 100 ms). White arrows in Fig 1(a) indicate the scan direction. Fe, Ti, and O atoms of the structural model (inner upper schemes) are illustrated in violet, gray, and red, respectively.

At higher energy resolution, EELS can probe electronic structure and local bonding environments; in particular, the $L_{2,3}$ edges provide information on the oxidation states of transition metals [22]. Figures 1(c)–1(e) present the evolution of Fe $L_{2,3}$ edges along different Fe-rich and mixed Fe-Ti atomic sites and thus map the valence distribution in the FTO phase. The elemental mapping in Fig. 1(b) enables one to identify the position of the Fe-rich (site A) and the mixed Fe-Ti (site B) atomic columns. Figure 1(f) shows typical experimental Fe $L_{2,3}$ spectra acquired on each type of site. The site A spectrum has an Fe L_3 edge maximum located at around 1.5 eV lower in energy than that of site B. Moreover, the present energy resolution can distinguish different multiplet features, which tend to vary in relative contributions depending on the formal valence state [33,34]. Each spectrum was therefore fitted with typical Fe^{2+} and Fe^{3+} reference spectra to quantify locally the valence state [34,35]. Linear combinations of the reference

spectra considered as individual components were used to fit each experimental spectrum, leading to the Fe^{2+} and Fe^{3+} reconstructed maps and the Fe^{2+}:Fe^{3+} ratio map displayed in Figs. 1(c)–1(e), respectively. While the Fe^{3+} contribution is relatively homogenous in intensity for both types of sites (with slight variations due to local elemental heterogeneities), the presence of Fe^{2+} is strongly modulated, with evident larger contributions on the Fe-rich sites [Fig. 1(c)]. This real-space valence mapping provides the experimental evidence of a Fe^{2+} and Fe^{3+} charge ordering at room temperature in the $R\bar{3}$ FTO phase. Estimated Fe^{2+}:Fe^{3+} ratios increase to a maximum of around 2.1 on the Fe-rich sites and around 1.2 on the mixed Fe-Ti sites. These estimations indicate a general tendency of the valence distributions and have to be considered as only semiquantitative, because of the potential intermixing of inelastic EELS signal due to possible effects of delocalization when using a subangstrom electron beam (see the Supplemental Material [29]). Tan *et al.* previously investigated that fundamental issue on a model system, i.e., Mn_3O_4, by mapping the Mn^{2+}-Mn^{3+} valence state distributions, and concluded that there was an underestimation of the determined valence state variations corroborated with quantitative simulations [25]. In our case, intermixing will lead to both cationic and charge orderings underestimations. In addition, high-resolution EELS spectra extracted at the Ti $L_{2,3}$ edges indicate only the presence of Ti^{4+} [29]. From all these experimental findings, the valence distribution can be summarized as follows: a main Fe^{2+}-Fe^{3+} ordering on A sites alternating with Ti^{4+}-Fe^{2+}-Fe^{3+} ordering on B sites, with a major Fe^{2+} contribution on both sites. Coming back to the stoichiometric $Fe_{1.35}Ti_{0.65}O_3$ phase, a simple electronegativity calculation (assuming solely Ti^{4+}) leads to a $Fe^{2+}_{0.65}Fe^{3+}_{0.70}Ti^{4+}_{0.65}O^{2-}_3$ valence distribution, i.e., Fe^{2+}:Fe^{3+} = 0.92. However, our experimental results present a much larger Fe^{2+}:Fe^{3+} ratio despite the potential intermixing effects. Such discrepancy may originate either from the presence of oxygen vacancies or from large Fe/Ti fluctuations. Here additional experimental work has been undertaken to clarify this point: (i) the oxygen content determined by Rutherford backscattering spectrometry (RBS) measurements yields $\delta = 0.35$ (0.15) across the overall FTO film, corroborating the general presence of oxygen vacancies, this is further confirmed since larger electrical conductivity values are reported in these films when grown under low oxygen partial pressure conditions [16,27]; (ii) although fine cationic heterogeneities were observed at the atomic scale, they do not apparently impact on the Fe^{2+}:Fe^{3+} ratio distribution (see the Supplemental Material [29]). All these considerations reveal the need to investigate deeper the influence of oxygen vacancies on the valence state distribution.

Hence, DFT calculations within the GGA + U approach have been used to interpret better the charge modulations

evidenced on the Fe atoms along the c axis in the ordered FTO phase. To have acceptable supercell sizes and reasonable calculation times, we investigate the commensurate structure, i.e., $Fe_{1.5}Ti_{0.5}O_3$, with an Fe:Ti ratio fairly close to that of the studied film. Figure 2(a) represents the distribution of the Fe oxidation states in the stoichiometric $Fe_{1.5}Ti_{0.5}O_3$ system. The supercell considered for the present calculation contains 36 Fe (24 Fe^{3+} and 12 Fe^{2+}), 12 Ti, and 72 oxygen atoms. The structure is ferrimagnetic, resulting from alternation between pure Fe layers with a mixed Fe^{2+}-Fe^{3+} contribution, and mixed Fe-Ti layers corresponding to Fe^{3+} and Ti^{4+} cations. The resulting electronic structure considered in this stoichiometric model does not agree with our previous experimental findings. Fig. 2(b) presents the atomic structure when a single oxygen vacancy is formed in the $Fe_{1.5}Ti_{0.5}O_{3-\delta}$ supercell with the oxygen vacancy site indicated. The energy cost of forming this oxygen vacancy is 3 eV, which is more favorable than in rutile, for example [36]. Several oxygen vacancy sites in this supercell were examined and all have formation energies of around 3 eV. The distribution of Fe oxidation states in the layers around the oxygen vacancy site is presented in Fig. 2(c). When a neutral oxygen vacancy is formed, the two electrons released can be transferred either to Fe or to Ti atoms, reducing (i) Fe^{3+} to Fe^{2+} or (ii) Ti^{4+} to Ti^{3+}. The most energetically favored structure is that in which two Fe^{3+} sites—one site in the Fe^{3+}-Ti^{4+} layer neighboring the vacancy and the other in the Fe^{3+}-Fe^{2+} layer neighboring the vacancy—are reduced to Fe^{2+}, i.e., an Fe^{2+}-Fe^{2+}-Fe^{3+} and Ti^{4+}-Fe^{3+}-Fe^{2+} charge ordering. Indeed, if one oxygen vacancy is present between every pair of cation planes, and if this vacancy injects electrons equally on both adjacent planes, the cation or charge ordering becomes ($2Fe^{3+}$-$2Fe^{2+}$-$4Ti^{4+}$) for the Fe and Ti mixed plane and ($2Fe^{3+}$-$6Fe^{2+}$) for the Fe-rich plane. This finding is in fair agreement with the
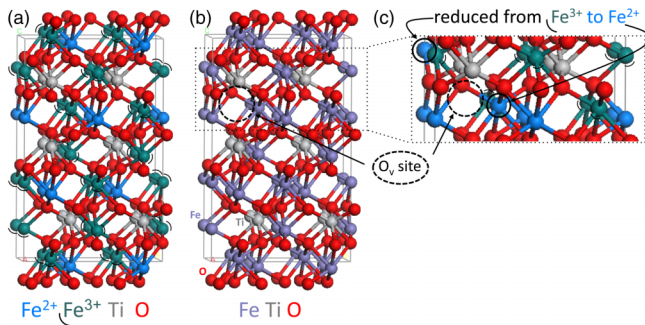
STEM-EELS results obtained on the FTO films, where a strong Fe^{2+} modulation is observed between Fe-rich and Fe-Ti mixed planes, while the Fe^{3+} distribution remains almost equivalent in both planes. Such a valence distribution corresponds to one oxygen vacancy between every cationic plane, i.e., 6 oxygen vacancies in the supercell presented in the Fig. 2(a). Based on the DFT calculations, the estimated oxygen vacancy implies $\delta = 3 - (72 - 6)/72 \times 3 = 0.25$, which is fairly close to the RBS measurements giving $\delta = 0.35$ (0.15). Hence, a significant level of oxygen vacancy levels must be considered as a major factor inducing the observed Fe^{2+}:Fe^{3+} ratio, and preserving the charge ordering despite local elemental heterogeneities.

Finally, physical macroscopic properties have been determined for the FTO thin film by both macroscopic magnetization and electrical conductivity measurements. Figure 3(a) presents the magnetic field dependence of magnetization measured at 10 and 300 K with magnetic field along the film plane. Hysteresis loops describe a solely magnetic phase, with significant magnetization at room temperature. The experimental saturation magnetization value at 10 K is equal to $M_s = 1.33 \mu_B$/formula. Based on the valence state distribution determined by STEM-EELS and supported by DFT calculations including oxygen vacancies, one can deduce in the commensurate $Fe_{1.5}Ti_{0.5}O_{3-\delta}$ the following valence state distributions on adjacent planes: (Fe^{2+}-Fe^{3+}-Fe^{2+}-Fe^{2+}) and (Ti^{4+}-Fe^{2+}-Ti^{4+}-Fe^{3+}). Assuming an AFM coupling between such planes, and a FM coupling between in-plane Fe ions, as found for the end members, magnetization per formula unit in commensurate $Fe_{1.5}Ti_{0.5}O_{3-\delta}$ can be calculated in the simplest ionic superexchange model (considering Fe^{3+} with $5\mu_B$, Fe^{2+} with $4\mu_B$, and $0\mu_B$ for "$3d^0$" Ti^{4+}). The resulting theoretical magnetization per formula unit is $[3\mu(Fe^{2+}) + \mu(Fe^{3+})] - [\mu(Fe^{2+}) + \mu(Fe^{3+})] = 8\mu_B$/4formula $= 2\mu_B$/formula. This theoretical value predicted for the $Fe_{1.5}Ti_{0.5}O_{3-\delta}$ phase has

FIG. 2 (color online). (a) Fe oxidation state distributions in $Fe_{1.5}Ti_{0.5}O_3$ (Ti atoms are all Ti^{4+}), (b) $Fe_{1.5}Ti_{0.5}O_{3-\delta}$ model including a single oxygen vacancy, (c) distribution of Fe oxidation states in the two layers around the oxygen vacancy site. In all figures, Ti atoms are labeled in gray and O in red. In (b) Fe atoms are in violet while in (a) and (c) Fe^{2+} and Fe^{3+} are in blue and green, respectively. Additionally in (a) and (c), Fe^{3+} are marked by a quarter circle to distinguished from Fe^{2+} cations.

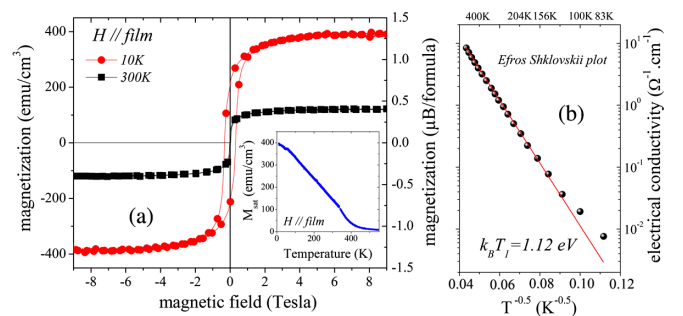

FIG. 3 (color online). (a) Magnetic field dependence of magnetization at 10 and 300 K (circles and squares, respectively) for the $Fe_{1.35}Ti_{0.65}O_{3-\delta}$ films, inset: temperature dependence of the saturation magnetization (magnetic field along the film plane). (b) Temperature dependence of the dc electrical conductivity (black dots) fitted with an Efros-Shklovskii (ES) model at $T > 100$ K (red line), the upper x axis is the temperature (in K).

never been observed, neither in bulk polycrystals [9], nor in thin films [14]. The discrepancy with experimental magnetization values can be attributed to the existence of crystalline twin boundaries, which are easily formed in the $Fe_{2-x}Ti_xO_3$ system [32]. Considering the cationic non-stoichiometry determined by the STEM-EELS study, i.e., $Fe_{1.35}Ti_{0.65}O_{3-\delta}$, a strong decrease in the theoretical magnetization is expected below $1\mu_B$/formula. Moreover, the Curie temperature, an intrinsic magnetic feature determined by the temperature dependence of magnetization [Fig. 3(a) inset] is found at $T_c = 420 \pm 20$ K, which is coherent with the experimental value in $Fe_{1.35}Ti_{0.65}O_{3-\delta}$ bulk ordered materials [8]. The temperature dependence of dc-electrical conductivity $\sigma(T)$, with a film in-plane current, presents a semiconducting behavior for 80 K $< T <$ 530 K [Fig. 3(b)]; no peculiar feature is observed at T_c. To understand better the conduction regime, the thermally activated behavior $\sigma(T)$ was fitted using different models: Arrhenius law, nearest-neighbor hopping, Mott variable range hopping, and the Efros-Shklovskii variable range hopping (ESVRH). The ESVRH, i.e., $\ln\{\sigma(T) = \sigma_0 \exp[-(T_1/T)^{0.5}]\}$ versus $T^{-1/2}$ [Fig. 3(c)], yields the best fit to the present experimental data (see the Supplemental Material [29] and Ref. [37]). The ESVRH mechanism is associated with an electron hopping from one site to another as in Mott variable range hopping, but introducing electronic correlations related to Coulomb interactions [38]. The T_1 parameter (where $k_B T_1 =$ 1.12 eV) determines the carrier localization length $\xi = (2.8e^2/\varepsilon_0\varepsilon_r k_B T_1) \approx 1.19$ nm, the hopping distance $R_{hop} = 0.25\xi(T_1/T) \approx 12.9$ nm, and the average hopping energy $W_{hop} = 0.5k_B(T_1 T)^{1/2} \approx 85$ meV [29,39]. These values are coherent with an ESVRH model, since R_{hop} is much higher than the nearest neighbor distance between Fe in planes, typically around 0.3 nm for the end members [40], and W_{hop} presents a lower value than the activation energy estimated from the Arrhenius model ($E_A =$ 0.14 eV). In addition, the STEM-EELS experiments reveal in the studied FTO film the presence of only one mixed-valence state, i.e., Fe^{2+} and Fe^{3+}, with solely nonmagnetic Ti^{4+}. This finding highlights a charge carrier transport mechanism taking place using only Fe^{2+}-Fe^{3+} hopping centers, which are characterized by strong electronic correlations [37]. Hence, we evidence that the conduction regime in these systems originates only from the Fe^{2+}-Fe^{3+} mixed-valence state, as earlier proposed by Ishikawa *et al.* for $Fe_{2-x}Ti_xO_3$ polycrystals [9] and followed later [41], but never directly demonstrated for high Ti composition ($x \geq 0.5$) to date.

In this Letter, we reveal by atomically resolved electron spectromicroscopy experiments, i.e., by STEM-EELS, the presence of a cationic ordering in oxygen deficient $Fe_{1.35}Ti_{0.65}O_{3-\delta}$ thin films at the atomic plane level. More interestingly, this real-space technique enables us to evidence for the first time the Fe^{2+}-Fe^{3+} charge ordering at room temperature characterized by a strong modulation of the Fe^{2+} distribution along the c axis. DFT calculations predict the presence of Fe^{2+} only in the Fe-rich planes for the stoichiometric model. Inclusion of oxygen vacancies reveals an overall charge distribution in better agreement with the experimental STEM-EELS results, i.e., (i) Fe^{2+} ions are preferentially localized on Fe-rich planes, (ii) a larger Fe^{2+} contribution than expected is estimated on both sites, while (iii) titanium remains Ti^{4+}. Finally, the macroscopic magnetic and transport properties of $Fe_{1.35}Ti_{0.65}O_{3-\delta}$ thin films are newly interpreted based on these experimental and theoretical findings. The charge distribution mechanism influences strongly the saturation magnetization, while exchange interactions, as probed with T_c, are not affected. The observed charge transport hopping mechanism is coherent with a charge ordering at room temperature and arises originating solely from the Fe^{2+}-Fe^{3+} mixed-valence state. Hence, the present results emphasizing the Fe^{2+} and Fe^{3+} variations and the key role of oxygen vacancies will certainly stimulate further *ab initio* calculations as well as guide the elaboration of new homogeneous artificial $Fe_{2-x}Ti_xO_{3-\delta}$ thin films [42] or even $(Fe_2O_3/FeTiO_3)_n$ superlattices [12,43].

---

*To whom correspondence should be addressed.
yves.dumont@uvsq.fr

[1] J. G. Bednorz and K. A. Müller, Z. Phys. B **64**, 189 (1986).
[2] M. Imada, A. Fujimori, and Y. Tokura, Rev. Mod. Phys. **70**, 1039 (1998).
[3] I. Terasaki, Y. Sasago, and K. Uchinokura, Phys. Rev. B **56**, R12685 (1997).
[4] N. A. Hill, J. Phys. Chem. B **104**, 6694 (2000); W. Eerenstein, N. D. Mathur, and J. F. Scott, Nature (London) **442**, 759 (2006).
[5] A. Ohtomo and H. Y. Hwang, Nature (London) **427**, 423 (2004).

[6] S. Thiel, G. Hammer, A. Schmehl, C. W. Schneider, and J. Mannhart, Science **313**, 1942 (2006); S. Valencia, A. Crassous, L. Bocher, V. Garcia, X. Moya, R. O. Cherifi, C. Deranlot, K. Bouzehouane, S. Fusil, A. Zobelli, A. Gloter, N. D. Mathur, A. Gaupp, R. Abrudan, F. Radu, A. Barthélémy, and M. Bibes, Nat. Mater. **10**, 753 (2011).

[7] L. Bocher, A. Gloter, A. Crassous, V. Garcia, K. March, A. Zobelli, S. Valencia, S. Enouz-Vedrenne, X. Moya, N. D. Mathur, C. Deranlot, S. Fusil, K. Bouzehouane, M. Bibes, A. Barthélémy, C. Colliex, and O. Stéphan, Nano Lett. **12**, 376 (2012).

[8] Y. Ishikawa and S. Akimoto, J. Phys. Soc. Jpn. **12**, 1083 (1957).

[9] Y. Ishikawa, J. Phys. Soc. Jpn. **13**, 37 (1958).

[10] R. J. Harrison, T. Kasama, T. A. White, E. T. Simpson, and R. E. Dunin-Borkowski, Phys. Rev. Lett. **95**, 268501 (2005).

[11] W. H. Butler, A. Bandyopadhyay, and R. Srinivasan, J. Appl. Phys. **93**, 7882 (2003).

[12] R. Pentcheva and H. Sadat Nabi, Phys. Rev. B **77**, 172405 (2008).

[13] H. Hojo, K. Fujita, K. Tanaka, and K. Hirao, Appl. Phys. Lett. **89**, 082509 (2006); **89**, 142503 (2006).

[14] A. Hamie, E. Popova, Y. Dumont, E. Chikoidze, B. Warot-Fonrose, B. Berini, and N. Keller, Appl. Phys. Lett. **98**, 232501 (2011); A. Hamie, Y. Dumont, E. Popova, J. Scola, A. Fouchet, B. Berini, and N. Keller, J. Appl. Phys. **108**, 093710 (2010).

[15] Z. Dai, N. Naramoto, K. Narumi, S. Yamamoto, and A. Miyashita, J. Appl. Phys. **85**, 7433 (1999); F. Zhou, S. Kotru and R. K. Pandey, Thin Solid Films **408**, 33 (2002).

[16] H. Ndilimabaka, Y. Dumont, E. Popova, P. Desfonds, F. Jomard, N. Keller, M. Basletic, K. Bouzehouane, M. Bibes, and M. Godlewski, J. Appl. Phys. **103**, 07D137 (2008).

[17] N. E. Brown, A. Navrotsky, G. L. Nord, Jr., and S. K. Banerjee, Am. Mineral. **78**, 941 (1993).

[18] L. M. Sandratskii and J. Kübler, Europhys. Lett. **33**, 447 (1996); I. Dzyaloshinsky, J. Phys. Chem. Solids **4**, 241 (1958); T. Moriya, Phys. Rev. **120**, 91 (1960).

[19] P. F. McDonald, A. Parasiris, R. K. Pandey, B. L. Gries, and W. P. Kirk, J. Appl. Phys. **69**, 1104 (1991).

[20] O. L. Krivanek, M. F. Chisholm, V. Nicolosi, T. J. Pennycook, C. J. Corbin, N. Delby, M. F. Murfitt, C. S. Own, Z. S. Szilagyi, M. P. Oxley, S. T. Pantelides, and S. J. Pennycook, Nature (London) **464**, 571 (2010).

[21] M. Bosman, V. J. Keast, J. L. Garcia-Munoz, A. J. D'Alfonso, S. D. Findlay, and L. J. Allen, Phys. Rev. Lett. **99**, 086102 (2007); D. A. Muller, L. Fitting Kourkoutis, M. Murfitt, J. H. Song, H. Y. Hwang, J. Silcox, N. Dellbyand, and O. L. Krivanek, Science **319**, 1073 (2008).

[22] G. A. Botton, MRS Bull. **37**, 21 (2012).

[23] S. Turner, R. Egoavil, M. Batuk, A. A. Abakumov, J. Hadermann, J. Verbeeck, and G. Van Tendeloo, Appl. Phys. Lett. **101**, 241910 (2012); J. A. Mundy, G. Mao, C. M. Brooks, D. Schlom, and D. A. Muller, Appl. Phys. Lett. **101**, 042907 (2012).

[24] A. Torres-Pardo, A. Gloter, P. Zubko, N. Jecklin, C. Lichtensteiger, C. Colliex, J. M. Triscone, and O. Stéphan, Phys. Rev. B **84**, 220102 (2011).

[25] H. Tan, S. Turner, E. Yücelen, J. Verbeeck, and G. Van Tendeloo, Phys. Rev. Lett. **107**, 107602 (2011).

[26] J. M. Tomczak and S. Biermann, Phys. Status Solidi A **246**, 1996 (2009); J. M. Tomczak, F. Aryasetiawan, and S. Biermann, Phys. Rev. B **78**, 115103 (2008).

[27] E. Popova, B. Warot-Fonrose, H. Ndilimabaka, M. Bibes, N. Keller, B. Berini, K. Bouzehouane, and Y. Dumont, J. Appl. Phys. **103**, 093909 (2008); E. Popova, H. Ndilimabaka, B. Warot-Fonrose, M. Bibes, N. Keller, B. Berini, F. Jomard, K. Bouzehouane, and Y. Dumont, Appl. Phys. A **93**, 669 (2008).

[28] E. Popova, B. Warot-Fonrose, F. Bonell, S. Andrieu, Y. Dumont, B. Berini, A. Fouchet, and N. Keller, Surf. Sci. **605**, 1043 (2011).

[29] See Supplemental Material at http://link.aps.org/supplemental/10.1103/PhysRevLett.111.167202 for details on the sample growth preparation, the structural characterization, the STEM-EELS experimental details and the related data analysis, the DFT calculations details, and the electrical properties analysis.

[30] V. I. Anisimov, J. Zaanen, and O. K. Andersen, Phys. Rev. B **44**, 943 (1991); S. L. Dudarev, G. A. Botton, S. Y. Savrasov, C. J. Humphreys, and A. P. Sutton, Phys. Rev. B **57**, 1505 (1998).

[31] G. Kresse and J. Hafner, Phys. Rev. B **49**, 14251 (1994); G. Kresse and J. Furthmüller, Comput. Mater. Sci. **6**, 15 (1996).

[32] H. Hojo, K. Fujita, T. Mizoguchi, K. Hirao, I. Tanaka, K. Tanaka, and Y. Ikuhara, Phys. Rev. B **80**, 075414 (2009).

[33] C. Colliex, T. Manoubi, and C. Ortiz, Phys. Rev. B **44**, 11 402 (1991).

[34] S.-Y. Chen, A. Gloter, A. Zobelli, L. Wang, C.-H. Chen, and C. Colliex, Phys. Rev. B **79**, 104103 (2009).

[35] G. Radtke, S. Lazar, and G. A. Botton, Phys. Rev. B **74**, 155117 (2006).

[36] B. J. Morgan and G. W. Watson, J. Phys. Chem. C **114**, 2321 (2010).

[37] Y. Dumont et al. (unpublished).

[38] A. Efros, J. Phys. C **9**, 2021 (1976); A. Efros and B. Sklovskii, J. Phys. C **8**, L49 (1975); B. I. Shklovskii and A. L. Efros, *Electronic Properties of Doped Semiconductor* (Springer-Verlag, Berlin, 1984).

[39] L. W. Finger and R. M. Hazen, J. Appl. Phys. **51**, 5362 (1980).

[40] J. Adkins, J. Phys. Condens. Matter **1**, 1253 (1989); B. A. Wechsler and C. T. Prewitt, Am. Mineral. **69**, 176 (1984).

[41] Y. Takada, M. Nakanishi, T. Fujii, and J. Takada, J. Magn. Magn. Mater. **310**, 2108 (2007).

[42] E. Chikoidze, T. Tchelidze, E. Popova, P. Maso, N. Ponjavidze, N. Keller, and Y. Dumont, Appl. Phys. Lett. **102**, 122112 (2013).

[43] H. Sadat Nabi, R. J. Harrison, and R. Pentcheva, Phys. Rev. B **81**, 214432 (2010).